Kinetic and Thermodynamic Control in Rare Earth Cyamelurates Synthesis

Albina S. Isbjakowa
Lomonosov Moscow State University Department of Chemistry: Moskovskij gosudarstvennyj universitet imeni M V Lomonosova Himiceskij fakul'tet

Vladimir V. Chernyshev
Lomonosov Moscow State University Department of Chemistry: Moskovskij gosudarstvennyj universitet imeni M V Lomonosova Himiceskij fakul'tet

Victor A. Tafeenko
Lomonosov Moscow State University Department of Chemistry: Moskovskij gosudarstvennyj universitet imeni M V Lomonosova Himiceskij fakul'tet

Leonid A Aslanov (aslanov.38@mail.ru)
Lomonosov Moscow State University Department of Chemistry: Moskovskij gosudarstvennyj universitet imeni M V Lomonosova Himiceskij fakul'tet https://orcid.org/0000-0002-0614-2902

Research Article

Keywords: cyamelurates, crystal structure, kinetic control, thermodynamic control, rare-earth elements

Posted Date: October 21st, 2021

DOI: https://doi.org/10.21203/rs.3.rs-989504/v1

Abstract

If various compounds exist in the metal cation – $C_6N_7O_3^{3-}$ – H_2O system, the synthesis temperature can affect the isolation of a particular product. Low temperatures favor the release of metastable kinetic products, and high temperatures, on the contrary, of thermodynamic ones. It is found that several structural types exist in the row of rare-earth cyamelurates. Room temperature synthesis leads to the formation of $[Ln(H_2O)_7C_6N_7O_3]$ (Ln=Y, Pr, Nd, Sm, Eu, Gd, Tb, Dy, Ho, Er), an increase in temperature yields thermodynamically more stable $[Ln(H_2O)_4C_6N_7O_3]_n \cdot nH_2O$ (Ln=Y, Ho, Er, Tm, Yb, Lu) and $[Ln(H_2O)_5C_6N_7O_3]_n$ (Ln = Pr, Nd). The change in the synthesis temperature did not affect the structures of Sm, Eu, Gd, Tb, Dy cyamelurates, as well as the structure of lanthanum cyamelurate $[La(H_2O)_6C_6N_7O_3] \cdot H_2O$.

In synthesized at increased temperature $[Ln(H_2O)_4C_6N_7O_3]_n \cdot nH_2O$ and $[Ln(H_2O)_5C_6N_7O_3]_n$ cyamelurates polymeric chains exist due to the fact that the cyamelurate anion acts as a bridging ligand. Kinetically trapped Y, Pr, Nd, Ho, Er cyamelurates, in contrast, consist of individual complex molecules $[Ln(H_2O)_7C_6N_7O_3]$. Probably, steric difficulties caused a decrease in the coordination number of Y, Ho, Er from 9 to 8 in the thermodynamic product. The coordination number of Pr and Nd remains equal to 9 in both types of compounds.

Introduction

Heptazine-based compounds, mostly polymer melon (known as graphite-like carbon nitride *g*-C_3N_4), have gained great popularity in recent years due to their promising practical applications in catalysis, including photocatalysis, preparation of hybrid membranes, sensors, materials for bioimaging etc. [1–4]. Also noteworthy are compounds with monomeric analogs of heptazine, for example, with 2,5,8-trihydroxy-s-heptazine or cyameluric acid. Recently obtained metal-organic frameworks (MOFs) based on lanthanide ions and cyamelurate anion linkers showed high selectivity in the separation of a CO_2/CH_4 gas mixture [5]. In addition, cyameluric acid derivatives exhibit reversible chromic behaviour [6] and have thermal stability up to 500°C [7].

Metal cyamelurates are interesting not only because of their properties, but also due to the variety of substances that exist in the metal cation – cyamelurate anion – water system. By slightly changing the synthesis conditions, completely different products can be obtained. For example, we isolated manganese cyamelurate $KMn(C_6N_7O_3) \cdot 5H_2O$ [8], the composition and diffraction pattern of which is similar to the results of the work [9], but different from the crystals described in [6]. On the other hand, samples of cobalt cyamelurate synthesized in [9] and [8] are divers: energy dispersive spectroscopy indicates the absence of potassium cations in the cobalt cyamelurate sample [9], whereas in our case the composition corresponds to $KCo(C_6N_7O_3) \cdot 5H_2O$ [8]. Most likely, the reaction time, which was various in these three works, is the main parameter determining the synthesis of a particular substance.

Short reaction times as well as low temperatures are the main characteristics of kinetic control, allowing the isolation of metastable substances that precede the thermodynamically stable phase [10, 11]. Accordingly, long reaction times and high temperatures result in thermodynamically stable products. The diversity of metal cyamelurates can be explained from the point of view of kinetic and thermodynamic control. Low solubility of cyameluric acid salts, which complicates the dissolution-recrystallization processes, promotes the release of kinetic products, but at the same time complicates the study of their structures due to the absence of large single crystals and, frequently, due to the presence of other coprecipitating phases.

In our previous studies, most of the samples obtained at room temperature (i.e. under kinetic control) contained an impurity amorphous phase [8, 12]. This fact, as well as the difference in the structure and composition of zinc cyamelurates depending on the reaction time, allowed us to put forward a hypothesis about the nonclassical nucleation of crystals inside micelles surrounded by an electric double layer [12]. This hypothesis can also be applied to lanthanide melonates. It is clearly shown in the work [13] that the as-synthesized neodymium and praseodymium melonate precipitates contain an amorphous phase, and after a several days of aging at room temperature samples transform into phase isostructural to $LnC_6N_7(NCN)_3 \cdot 8H_2O$. The fraction of the amorphous phase during aging is significantly reduced, which is very similar to slow transformation of amorphous phase to crystalline one or crystal-amorphous-crystal phase transition [14].

One gets the impression that the isotypic rare-earth melonates $LnC_6N_7(NCN)_3 \cdot 8H_2O$ (Ln=La, Ce, Pr, Nd, Sm) are thermodynamically stable, since $LaC_6N_7(NCN)_3 \cdot 8H_2O$ crystals suitable for X-ray diffraction analysis can be grown by the slow diffusion technique (provides equilibration), and $LnC_6N_7(NCN)_3 \cdot 8H_2O$ (Ln=Nd, Pr) precipitate at a synthesis temperature of about 80 °C. In addition, $SmC_6N_7(NCN)_3 \cdot 8H_2O$ phase is formed under hydrothermal conditions using sample prepared at room temperature as starting material. The authors also note that kinetic products contain more water molecules and correspond to the composition $LnC_6N_7(NCN)_3 \cdot 12H_2O$ (Ln=Pr, Nd, Sm, Eu) [13]. But as in the case of metal cyamelurates obtained under kinetic control [8, 12], polycrystalline samples of lanthanide melonates did not contain crystals, large enough for single-crystal X-ray diffraction analysis. Therefore the structure of $LnC_6N_7(NCN)_3 \cdot 12H_2O$ is not solved.

Another example of thermodynamic control in synthesis of cyameluric acid salts is preparation of lanthanide MOFs [5]. Keeping the reaction mixture at 80°C for 24 hours followed by slow cooling resulted in a single-phase sample containing crystals of identical morphology, 50-150 μm in size. MOFs with common formula $[Ln(H_2O)_2C_6N_7O_3]_n$ (Ln=La, Ce, Pr) are isostructural and crystallize in the tetragonal $P4_322$ space group.

As in the case of lanthanide melonates, metastable cyamelurates are likely to exist, which can be isolated under kinetic control using room temperature and short reaction times. It is also interesting whether compounds similar to MOFs [5] can be obtained using increased temperatures but with the same reaction

time as in kinetic control synthesis. Therefore the aim of this work is synthesis and structural study of lanthanide cyamelurates obtained under kinetic and thermodynamic control.

Experimental

Materials

Melamine (99,8%, GE), KOH (puriss., Labtech), $Y(NO_3)_3 \bullet 6H_2O$(99,8%, Sigma-Aldrich), $La(NO_3)_3 \cdot 4(CH_3)_2SO$, Pr_2O_3, Nd_2O_3, Sm_2O_3, $EuCl_3 \cdot 6H_2O$(99,9%, Sigma-Aldrich), Gd_2O_3, Tb_2O_3, Dy_2O_3, Ho_2O_3, $ErCl_3 \bullet 6H_2O$(99,9%, Sigma-Aldrich), $Tm(NO_3)_3 \bullet 5H_2O$(99,9%, Sigma-Aldrich), $YbCl_3 \cdot 6H_2O$(99,9%, Sigma-Aldrich), $Lu(NO_3)_3 \bullet xH_2O$ (99,9%, Sigma-Aldrich).

Synthesis of melon

The bulk melon was prepared according to [15]. The final product is light-yellow powder: C, % - 34,73; H, % - 2,05; N, % - 61,79 (chemical formula $C_3N_{4,57}H_{2,12}$, which corresponds to the results of [16]).

Synthesis of potassium cyamelurate

Potassium cyamelurate ($K_3C_6N_7O_3$) was obtained by refluxing melon powder in aqueous KOH solution (2.5 molar) for several hours as described in [17]. The reaction mixture was exposed to hot filtration. After cooling to 0 ˚C colorless precipitatewas filtered and washed with ethanol, acetone and dried in air at 180 ˚C.

Synthesis of rare-earth chlorides

$PrCl_3$, $NdCl_3$, $SmCl_3$, $GdCl_3$, $TbCl_3$, $DyCl_3$, $HoCl_3$ were obtained in a similar way [18], using oxides instead of carbonates. The dissolution of oxides in hydrochloric acid was carried out upon moderate heating.

Synthesis of rare-earth cyamelurates

Dry potassium cyamelurate was used in the synthesis. To obtain cyamelurates of rare-earth metals either nitrates or chlorides of the corresponding elements were used. All reactions were carried out both at elevated and at room temperatures by adding a solution of potassium cyamelurate (concentration varied from 0.010 to 0.050 mol/L) to a solution of a rare-earth salt (concentration varied from 0.030 to 0.100 mol/L) upon stirring. The ratio Ln^{3+}:$C_6N_7O_3^{3-}$ in this case varied from 1:1 to 1.2:1. The synthesis time did not exceed 5 minutes and pH of the final solutions was approximately in interval 4–5. No dependence of product structures on the concentration and ratio of reagents as well as on composition of rare-earth precursor was found, but they are influenced by both the nature of the metal and the temperature. For details, see below. Samples obtained at room temperature are hereinafter designated as **Ln1**, at elevated temperature – **Ln2** (Ln = Y, La, Pr, Nd, Sm, Eu, Gd, Tb, Dy, Ho, Er, Tm, Yb, Lu).

Characterization

Powder X-ray Diffraction. Powder X-ray diffraction measurements were carried at ambient conditions at two laboratory diffractometers – Huber G670 Guinier camera ($CoK_{\alpha 1}$ radiation) and EMPYREAN (PANalytical, Ni-filtered CuK_{α} radiation). Data collection details for **Er1, Gd1, Pr1, Er2, Nd2 and La2** are given in Table S1. Unit cell dimensions were determined using three indexing programs: TREOR90 [18], ITO [20], and AUTOX [21, 22]. The unit cell parameters and space groups were tested with the use of the Pawley fit [23] and confirmed by the crystal structure solution. We came to the crystal structures for **Er1, Gd1, Pr1, Er2, Nd2 and La2** by using a simulated annealing technique [24]. The model used for the cyamelurate molecule, in a direct space search without H atoms, was taken from the literature [1]. A bond-restrained Rietveld refinement implemented within MRIA [25] was applied to the above results. In the refinements, preferred orientation approximated with a March-Dollase formalism [26] and anisotropic line broadening [27] were taken into account. H atoms in all structures were positioned geometrically (O–H 0.85–0.89 Å) and not refined. Rietveld plots for all structures after the final refinements are shown in Figures S8 – S13.

Crystal structures of **Er1, Gd1, Pr1, Er2, Nd2 and La2** were deposited in the Cambridge Structural Database [28], CCDC numbers are 2091700 – 2091705 respectively.

Chemical analysis turned out to be ineffective for determining the compositions of the obtained polycrystalline samples due to presence of unknown amorphous phase; therefore, the chemical compositions of the crystalline phases were determined solely by the results of X-ray diffraction analysis.

Results And Discussion

During the reaction of potassium cyamelurate with rare-earth salts, products are formed that can be divided into five groups:

1. Y1, **Pr1**, **Nd1**, **Sm1**, **Eu1**, **Gd1**, **Tb1**, **Dy1**, **Ho1**, **Er1** obtained at room temperature and **Sm2**, **Eu2**, **Gd2**, **Tb2**, **Dy2** obtained at elevated temperature (Fig. S1 – S3);

2. Tm1, **Yb1**, **Lu1** obtained at room temperature (Fig. S4);
3. Y2, **Ho2**, **Er2**, **Tm2**, **Yb2**, **Lu2** obtained at elevated temperature (Fig. S5);
4. Pr2 and **Nd2** obtained at elevated temperature (Fig. S6);
5. La1 and **La2** obtained at room and at elevated temperatures respectively (Fig. S7).
Within the group, the resulting products are isostructural; only for the second group of substances the structure has not been established. The main crystallographic characteristics for the solved structures **Er1, Gd1, Pr1, Er2, Nd2 and La2** are shown in Table S1. Since the substances in the group **Er1, Gd1, Pr1** are isostructural, only **Er1** structure is considered in detail below.

Er1 structure

The formula of erbium cyamelurate synthesized at room temperature can be represented as $[Er(H_2O)_7C_6N_7O_3]$, since **Er1** contains neutral complexes. The coordination number of metal atom is 9, it is

surrounded by 7 water molecules and is coordinated by the cyamelurate anion through the oxygen O2 and nitrogen N2 atoms (Fig. 1).

In the **Er1** structure, flat anions are arranged in stacks, which are displaced and rotated relative to each other by an angle of 180° (Fig. 2a). The distances between two neighbor anions in the stack are 3.19 Å and 3.36 Å (Fig. 2b). Adjacent stacks are arranged so that an angle of 34.13° is formed between the anions.

It is interesting to note that cyamelurate anions do not form endless chains typical for known cobalt(II) and cupper(II) cyamelurates [8], arising due to the polydentity of $C_6N_7O_3^{3-}$ anion, and hence the ability to act as a bridging ligand. Hydrogen bonds connect individual $[Er(H_2O)_7C_6N_7O_3]$ molecules together, and they are formed between all water molecules and oxygen and nitrogen atoms of the anion (except N1, N2, N4 atoms).

Er2 structure

The structure of erbium cyamelurate **Er2** obtained at elevated temperatures is shown in Figure 3.

Erbium atom is surrounded by 4 water molecules and is bound to two cyamelurate anions through the oxygen atoms O3, O2 and nitrogen atoms N5, N2 (coordination number is 8). The angle between the planar cyamelurate anions bound to the erbium cation is 75.26°. Such self-organization of alternating cations and bridging cyamelurate anions leads to endless undulating chains (Fig. 4a). The distance between planar anions of adjacent chains is 3.19 Å (Fig. 4b). Outer-sphere O8 water molecules are located between the chains. Although this complex is also neutral, but it consists of infinite polymer-like chains, therefore it can be represented by the formula $[Er(H_2O)_4C_6N_7O_3]_n \cdot nH_2O$.

Nd2 structure

The structure of neodymium cyamelurate **N2** obtained by boiling the reaction mixture is shown in the Figure 5.

In **Nd2** crystal structure, anions act as bridging ligands coordinating neodymium cation through oxygen O2, $O2^{i}$, $O3^{ii}$ and nitrogen $N2^{i}$ atoms (i = −x, 1−y, 1−z; ii = x, y, −1+z). Two coordination polyhedra have a common edge O2–$O2^{i}$ (Fig. 6a). Five water molecules complement the coordination sphere of neodymium (coordination number is 9). **Nd2** contains endless chains, $[Nd(H_2O)_5C_6N_7O_3]_n$, forming stacks of parallel cyamelurate anions, the distance between which is equal to 3,14 Å, two neodymium atoms are located between the stacks (Fig. 6b).

The chains are tied together by hydrogen bonds between nitrogen (except N1, N2) and oxygen atoms of anions and all five water molecules.

La2 structure

The structure of lanthanum cyamelurate is shown in Figure 7. The composition of **La2** based on structural data corresponds to the formula $[La(H_2O)_6C_6N_7O_3]\cdot H_2O$.

One lanthanum atom is coordinated by two cyamelurate anions through O1, $O1^{iv}$ and N2, $N2^{iv}$ atoms (where iv = x, –y, 0.5–z). Six water molecules complete the first coordination sphere. The coordination number of central atom is 10. One water molecule is located in the cavities formed between the stacks of anions and is held in the structure via hydrogen bonding O7–H7…O2, O7–H7…N3, $O4^{ii}$–$H4A^{ii}$…O7 (Fig. 7).

Neighboring lanthanum polyhedra have one common O1 vertex. Flat ribbons are realized in the structure (Fig. 8a). The ribbons are stacked (Fig. 8b), and the adjacent anions are located one above the other so that the distance between the ribbons displaced relative to each other is roughly equal to 3.3Å or 0.5*a*, where *a* – unit cell parameter.

Structure comparison

As in the case of lanthanide melonates [13], some rare-earth cyamelurates have different structures depending on the synthesis temperature. Both thermodynamic and kinetic products were isolated in the case of Nd, Pr,Y, Ho, Er, Tm, Yb, Lu cyamelurates.

Despite the variety of structures, it is possible to distinguish common features among kinetic and thermodynamic products. For example, the former contain single molecules $[Ln(H_2O)_7C_6N_7O_3]$ (Ln=Y, Pr, Nd, Ho, Er), the latter have endless polymer chains $[Ln(H_2O)_4C_6N_7O_3]_n$ (Ln=Y, Ho, Er, Tm, Yb, Lu), $[Ln(H_2O)_5C_6N_7O_3]_n$ (Ln=Nd, Pr), $[La(H_2O)_6C_6N_7O_3]_n$ formed due to the fact that the cyamelurate ion acts as a bridging ligand and binds neighboring cations. Also, metastable phases of lanthanide cyamelurates (as well as melonates [13]) contain more water molecules compared to thermodynamically stable ones.

In the case of yttrium and heavy lanthanides Ho and Er, the ion radius most likely affects the decrease in the coordination number from 9 to 8 with an increase in the reaction temperature. Since the central metal atom is surrounded by two large anions, and not one, as in the kinetic product, steric hindrances arise. The water molecule, which could be in the first coordination sphere, is held by hydrogen bonds in the second coordination sphere. On the other hand, the coordination number of neodymium and praseodymium cations is maintained as in the structure obtained at room temperature, although each atom is coordinated by three anions.

In each groups of isostructural complexes, from light to heavy lanthanides, the unit cell parameters decrease (Tables S2–S4), which is consistent with a lanthanide contraction. Also, powders of the first group, obtained at room temperature have unit cell parameters slightly less (by a few hundredths of an angstrom) as those synthesized at elevated temperatures.

Powders of samarium, europium, gadolinium, terbium, and dysprosium cyamelurates obtained both at room and elevated temperature have the same structure, isotypic to **Er1**. Therefore, this crystalline modification for the listed lanthanides is stable and rapidly forming, and this is the common case when

thermodynamic and kinetic products are the same [11]. This also applies to lanthanum cyamelurate, which differs from the other rare-earth cyamelurates presented in this work. On the other hand, it is possible that the boiling point of the reacting mixture is insufficient to obtain the most stable modification, and, as in the case of samarium melonate [13], hydrothermal conditions are required. However, our attempt to synthesize nickel cyamelurate under hydrothermal conditions led to the hydrolysis of the cyameluric acid residue [12]. For this reason, we abandoned this type of synthesis.

It is possible that nucleation of rare-earth cyamelurates, as well as zinc cyamelurates [12], takes place in colloidal electric double layer micelles formed in solution. Sequential complexation reactions occur inside such micelles. First, coordination of one anion to the cation aqua-complex lead to the gradual displacement of water molecules, and second, with an increase in temperature, the monomeric complex is transformed into polymeric one due to binding of neighboring monomers via polydentate bridging anions. The second stage also proceeds with the displacement of water molecules from the inner sphere of the complexes. This is clearly seen when comparing the structures of **Er1** and **Er2**, **Nd1** (isostructural to **Er1**) and **Nd2**.

The π–π stacking of anions in the crystal structures of different metal and ammonium cyamelurates was already mentioned in this article as well as in our previous ones [1, 8, 12]. Coulomb interactions between cations and anions and hydrogen bonds present in all obtained structures, but in $Ni(C_6N_7O_3H)\cdot 5H_2O$ [12] Coulomb interactions make a crucial contribution to the crystals potential energy; as a result, this crystal structure is a derivative of the CsCl-type structures (Fig. S14). Other studied structures (Fig. S15-S19) could not be attributed to known structural types, which is inevitable if Coulomb interactions exist not between individual cations and anions, but between ion aggregates collected in stacking columns under the influence of quadrupole [29] or diradicaloid interactions [30], as well as hydrophobic-hydrophilic balance. This means that relatively weak stacking effect can determine the type of crystal structure without a determinative contribution to the potential energy of crystals.

Conclusion

Lanthanide cyamelurates demonstrate the influence of kinetic and thermodynamic factors on crystal composition and structure, similar to the previously observed regularities [8, 12]. The assembly of cyamelurate anions into stacking columns generally determines the peculiarities of their interaction with cations and the formation of hydrogen bonds.

Declarations

Funding This work was financialy supported by Russian Foundation for Basic Research (grant 20-08-00097) and by M.V. Lomonosov Moscow State University Program of Development.

Conflicts of interest The authors have no conflicts of interest to declare that are relevant to the content of this article.

Data availability The datasets generated and analyzed during the current study are available in Cambridge Crystallographic Data Centre, CCDC numbers 2091700 – 2091705 for crystal structures of **Er1**, **Gd1**, **Pr1**, **Er2**, **Nd2** and **La2** respectively [https://www.ccdc.cam.ac. uk/].

Code availability not applicable

Author's contribution A. S. Isbjakowa, chemical syntheses and analyzes, writing of manuscript; V. V. Chernyshev, powder methods of crystal structure determinations V. A. Tafeenko, crystal-chemical analysis; L. A. Aslanov, setting a scientific problem and choosing objects of research, supervision of research, analysis of results.

Ethical approval All ethical standards mentioned in Instructions for Authors are fulfilled.

Consent to participate All authors agreed with participation in research and publication of the results.

Consent for publication All authors agreed with the content and all gave explicit consent to submit to Structural Chemistry Journal. All authors obtained consent from the responsible authorities at the institute/ organization where the work has been carried out, before submission. All listed authors have approved the manuscript before submission, including the names and order of authors.

References

1. Bushmeleva AS, Tafeenko VA, Zakharov VN, Lobova AL, Aslanov LA (2019) Ammonium cyamelurates: synthesis and crystalline structures. Struct Chem. https://doi.org/10.1007/s11224-018-1187-0
2. Ismael M (2020) A review on graphitic carbon nitride (g-C_3N_4) based nanocomposites: Synthesis, categories, and their application in photocatalysis. J Alloys Compd. https://doi.org/10.1016/j.jallcom.2020.156446
3. Krivtsov I, Mitoraj D, Adler Ch, Ilkaeva M, Sardo M, Mafra L, Neumann Ch, Turchanin A, Li Ch, Dietzek B, Leiter R, Biskupek J, Kaiser U, Im Ch, Kirchhoff B, Jacob T, Beranek R (2019) Water-Soluble Polymeric Carbon Nitride Colloidal Nanoparticles for Highly Selective Quasi-Homogeneous Photocatalysis. Angew Chem Int Ed. https://doi.org/10.1002/anie.201913331
4. Lau VW, Moudrakovski I, Botari T, Weinberger S, Mesch MB, Duppel V, Senker J, Blum V, Lotsch BV (2016) Rational design of carbon nitride photocatalysts by identification of cyanamide defects as catalytically relevant sites. Nat Commun. https://doi.org/10.1038/ncomms12165
5. Mohan M, Essalhi M, Durette D, Rana LK, Ayevide FK, Maris T, Duong A (2020) A rational design of microporous nitrogen-rich lanthanide metal–organic frameworks for CO_2/CH_4 separation. ACS Appl Mater Interfaces. https://doi.org/10.1021/acsami.0c15395
6. Mohan M, Rajak S, Tremblay AA, Maris T, Duong A (2019) Syntheses of mono and bimetallic cyamelurate polymers with reversible chromic behaviour. Dalton Trans. https://doi.org/10.1039/C9DT01278H

7. Horvath-Bordon E, Kroke E, Svoboda I, Fueß H, Riedel R, Neeraj S, Cheetham AK (2004) Alkalicyamelurates, $M_3[C_6N_7O_3]\cdot xH_2O$, M = Li, Na, K, Rb, Cs: UV-luminescent and thermally very stable ionic tri-s-triazine Derivatives. Dalton Trans. https://doi.org/10.1039/B412517G
8. Isbjakowa AS, Chernyshev VV, Tafeenko VA, Aslanov LA (2021) Metal cyamelurates: structural diversity caused by kinetic and thermodynamic controls. Struct Chem. https://doi.org/10.1007/s11224-021-01815-w
9. Holst JR (2009) Synthesis of inorganic heptazine-based materials. PhD thesis, University of Iowa, http://ir.uiowa.edu/etd/242
10. Kawano M, Haneda T, Hashizume D, Izumi F, Fujita M (2008) A Selective Instant Synthesis of a Coordination Network and Its Ab Initio Powder Structure Determination. Angew Chem Int Ed. https://doi.org/10.1002/anie.200704809
11. Ji Q, Lirag RC, Miljanic OS (2014) Kinetically controlled phenomena in dynamic combinatorial libraries. Chem Soc Rev. https://doi.org/10.1039/C3CS60356C
12. Isbjakowa AS, Chernyshev VV, Tafeenko VA, Shiryaev AA, Kudryavtsev IK, Aslanov LA (2021) Kinetic control of the zinc cyamelurate crystal formations. Struct Chem. https://doi.org/10.1007/s11224-020-01721-7
13. Makowski SJ, Schwarze A, Schmidt PJ, Schnick W (2012) Rare-Earth Melonates $LnC_6N_7(NCN)_3\cdot xH_2O$ (Ln = La, Ce, Pr, Nd, Sm, Eu, Tb; x = 8–12): Synthesis, Crystal Structures, Thermal Behavior, and Photoluminescence Properties of Heptazine Salts with Trivalent Cations. Eur J Inorg Chem. https://doi.org/10.1002/ejic.201101251
14. Bennett TD, Goodwin AL, Dove MT, Keen DA, Tucker MG, Barney ER, Soper AK, Bithell EG, Tan JC, Cheetham AK (2010) Structure and properties of an amorphous metal-organic framework. Phys Rev Lett. https://doi.org/10.1103/PhysRevLett.104.115503
15. Zhang W, Zhang Q, Dong F, Zhao Z (2013) The multiple effects of precursors on the properties of polymeric carbon nitride. Int J Photoenergy. https://doi.org/10.1155/2013/685038
16. Dyjak S, Kiciński W, Huczko A (2015) Thermite-driven melamine condensation to $C_xN_yH_z$ graphitic ternary polymers: towards an instant, large-scale synthesis of g-C_3N_4. J Mater Chem A. https://doi.org/10.1039/C5TA00201J
17. Braml NE, Schnick W (2013) New heptazine based materials with a divalent cation – $Sr[H_2C_6N_7O_3]_2\cdot 4H_2O$ and $Sr[HC_6N_7(NCN)_3]\cdot 7H_2O$. Z Anorg Allg Chem. https://doi.org/10.1002/zaac.201200345
18. Isbjakowa AS, Grigoriev MS, Golubev DV, Savinkina EV (2020) Synthesis and characterization of acetylurea complexes with rare-earth metal halides: Polymorphism of the praseodymium complexes. J Mol Struct. https://doi.org/10.1016/j.molstruc.2019.127141
19. Werner PE, Eriksson L, Westdahl M (1985) TREOR, a semiexhaustive trial-and-error powder indexing program for all symmetries. J Appl Crystallogr. https://doi.org/10.1107/S0021889885010512

20. Visser JW (1969) A fully automatic program for finding the unit cell from powder data. J Appl Crystallogr. https://doi.org/10.1107/S0021889869006649
21. Zlokazov VB (1992) MRIAAU - a program for autoindexing multiphase polycrystals. J Appl Crystallogr. https://doi.org/10.1107/S0021889891009366
22. Zlokazov VB (1995) AUTOX - a program for autoindexing reflections from multiphase polycrystal. Comput Phys Commun. https://doi.org/10.1016/0010-4655(94)00151-Q
23. Pawley GS (1981) Unit-cell refinement from powder diffraction scans. J Appl Crystallogr. https://doi.org/10.1107/S0021889881009618
24. Zhukov SG, Chernyshev VV, Babaev EV, Sonneveld EJ, Schenk H (2001) Application of simulated annealing approach for structure solution of molecular crystals from X-ray laboratory powder data. Z Krist. https://doi.org/10.1524/zkri.216.1.5.18998
25. Zlokazov VB, Chernyshev VV (1992) MRIA - a program for a full profile analysis of powder multiphase neutron-diffraction time-of flight (direct and Fourier) spectra. J Appl Crystallogr. https://doi.org/10.1107/S0021889891013122
26. Dollase WA (1986) Correction of intensities for preferred orientation in powder diffractometry: application of the March model. J Appl Crystallogr. https://doi.org/10.1107/S0021889886089458
27. Popa NC (1998) The (hkl) Dependence of diffraction-line broadening caused by strain and size for all Laue groups in Rietveld refinement. J Appl Crystallogr. https://doi.org/10.1107/S0021889897009795
28. Groom CR, Allen FH (2014) The Cambridge structural database in retrospect and prospect. Angew Chem Int Ed. https://doi.org/10.1002/anie.201306438
29. Hwang J, Li P, Shimizu KD (2017) Synergy between experimental and computational studies of aromatic stacking interactions. Org Biomol Chem. https://doi.org/10.1039/c6ob01985d
30. Kertesz M (2019) Pancake Bonding: An Unusual Pi-Stacking Interaction. Chem Eur J. https://doi.org/10.1002/chem.201802385

Figures

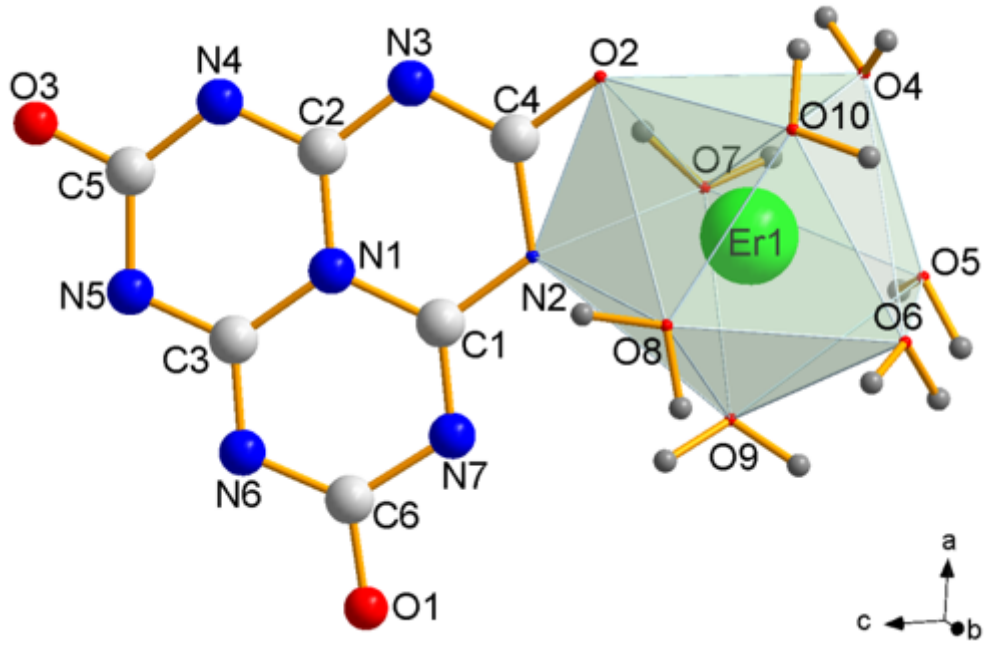

Figure 1

Struture of [Er(H2O)7C6N7O3]. Metal-ligand bonds are not shown for a more visual representation of the polyhedron

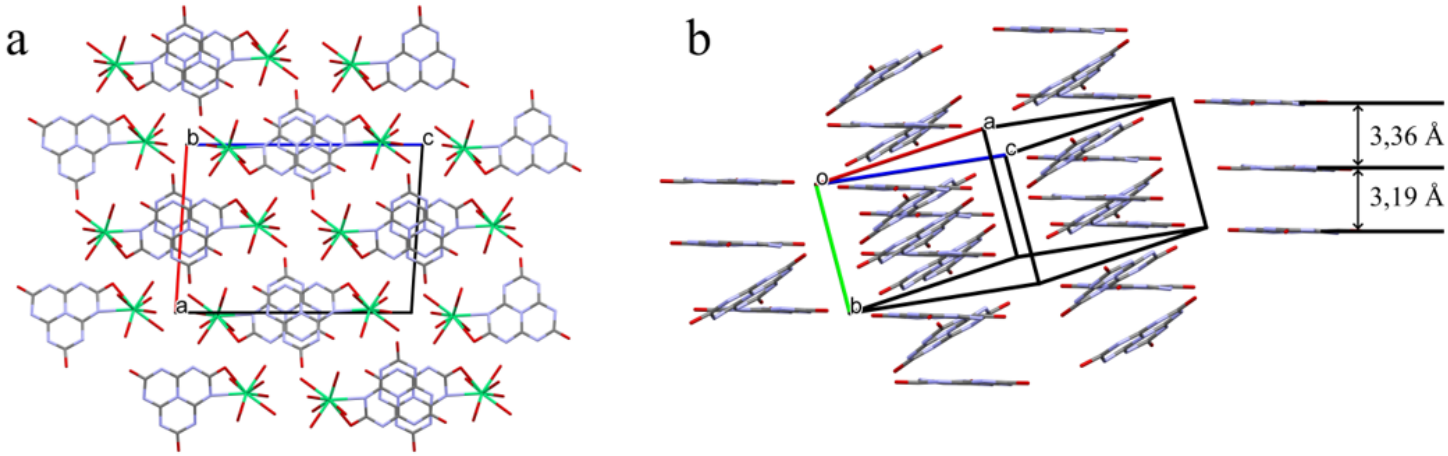

Figure 2

Stacks of cyamelurate anions in the Er1 structure, hydrogen atoms are not shown (a, b). Projection along the b-axis (a). Mutual orientations of cyamelurate anions (b)

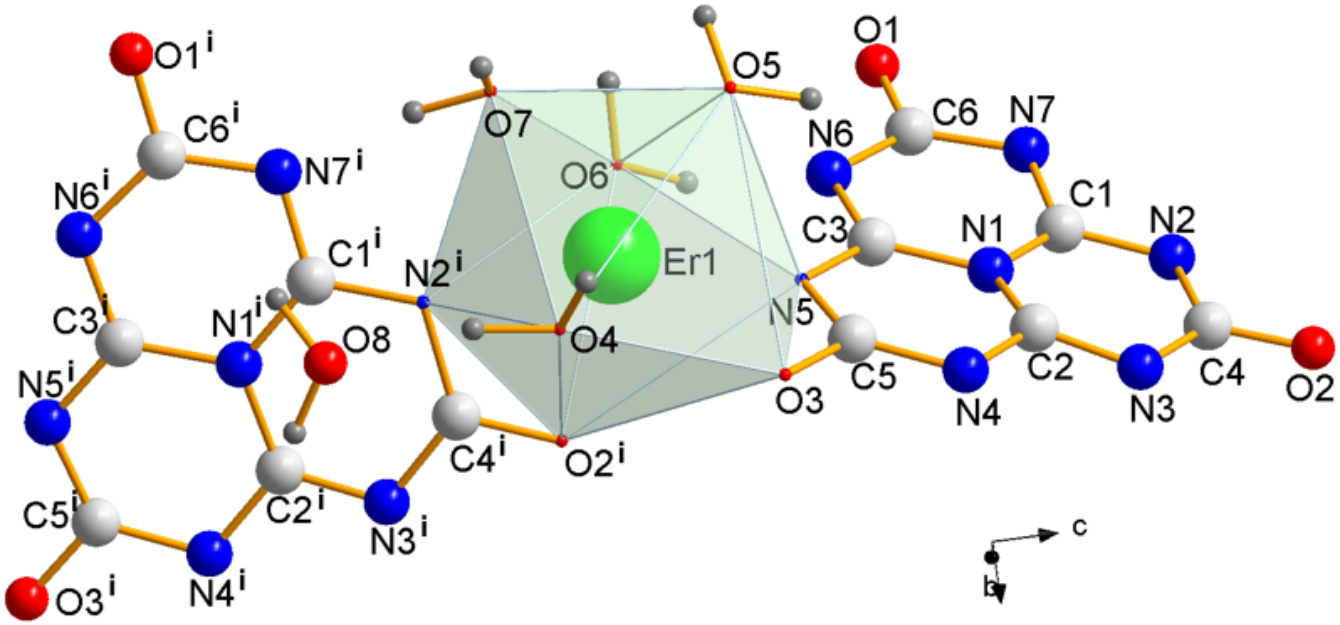

Figure 3

Atomic numbering and coordination environment of erbium atoms in the Er2 structure. Metal-ligand bonds are not shown for clarity. Symmetry code: i = x, 1−y, -0.5+z

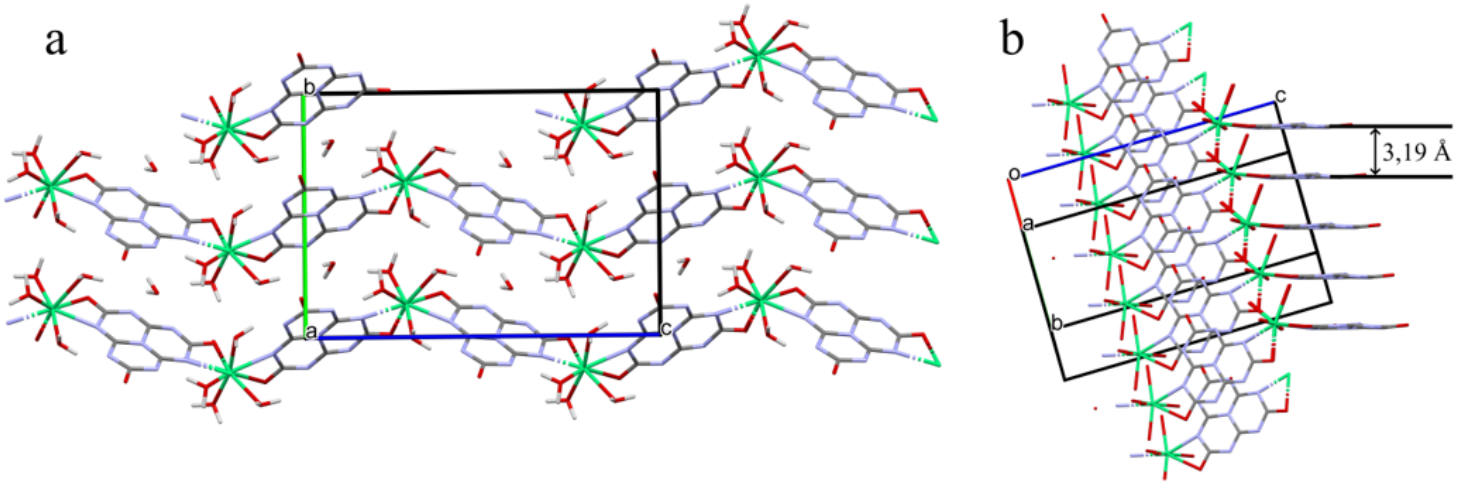

Figure 4

Infinite chains, projection along the a axis (a) and stacks of anions (hydrogen atoms are not shown) in the structure of [Er(H2O)4C6N7O3]n·nH2O (b)

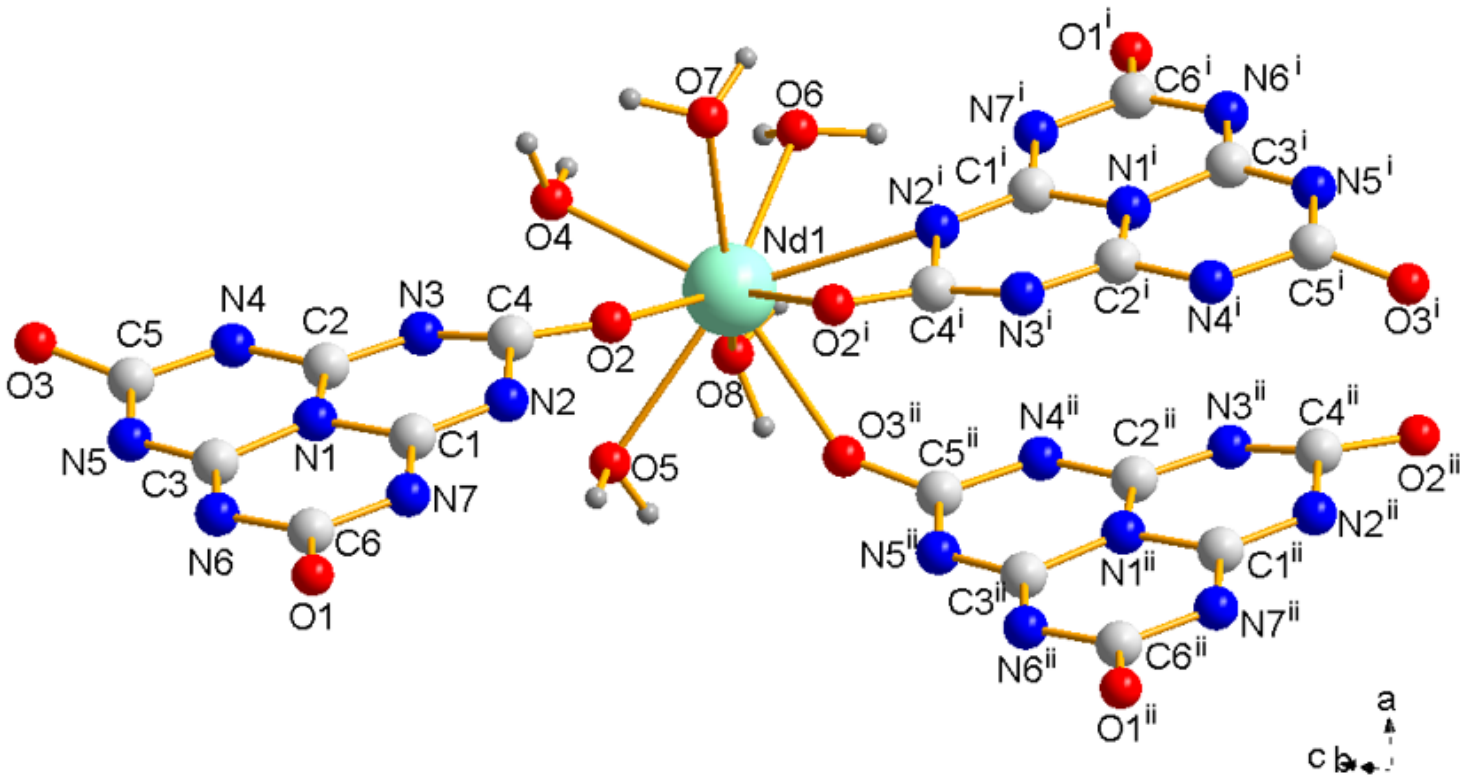

Figure 5

Numbering of atoms in a structure of Nd2. Symmetry codes: i = −x, 1−y, 1−z; ii = x, y, −1+z

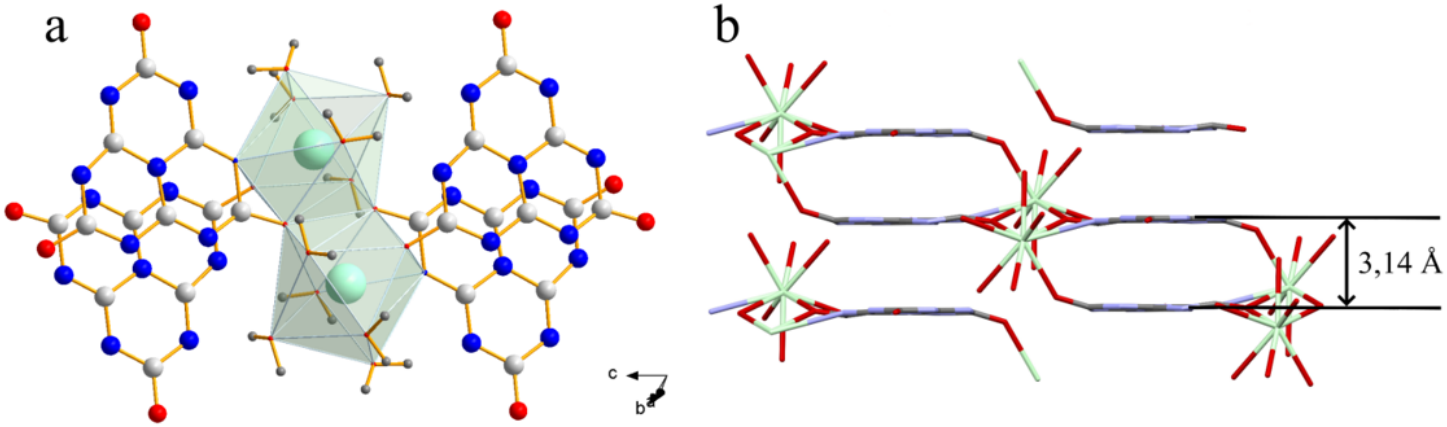

Figure 6

Two coordination polyhedra with a common O2–O2i edge (a). The arrangement of anions relative to each other in the structure, hydrogen atoms are not shown (b)

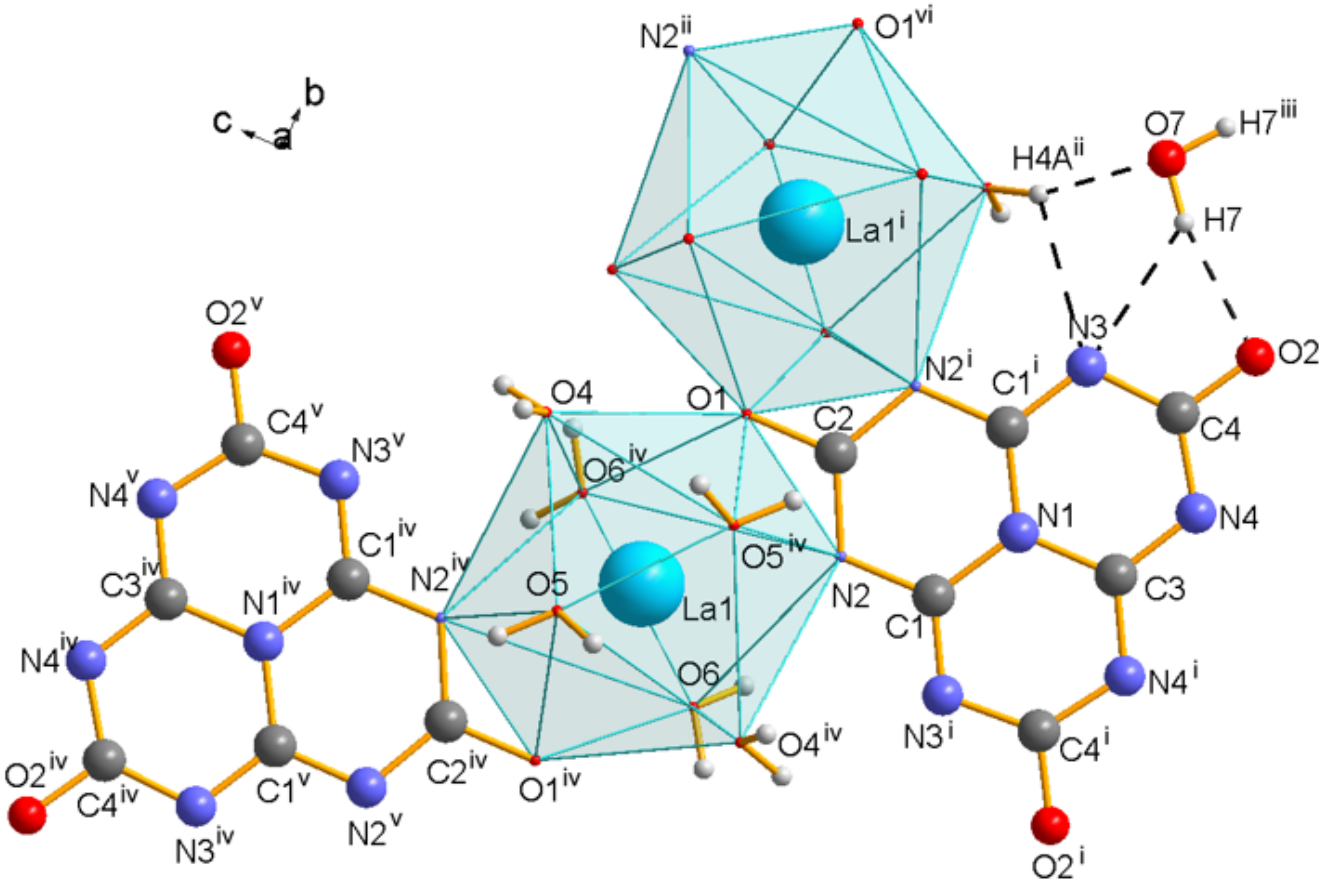

Figure 7

Structure of La2. For visual perception of the polyhedron, the coordination bonds of the central atom-ligand are not shown. Hydrogen bonds are indicated by black dashed lines. Symmetry codes: i=1−x, 0.5−y, z; ii=1−x, 0.5+y, 0.5−z; iii=1−x, 1.5−y, z; iv=x, −y, 0.5−z; v=1−x, −0.5+y, 0.5−z; vi=x, 1−y, 0,5−z

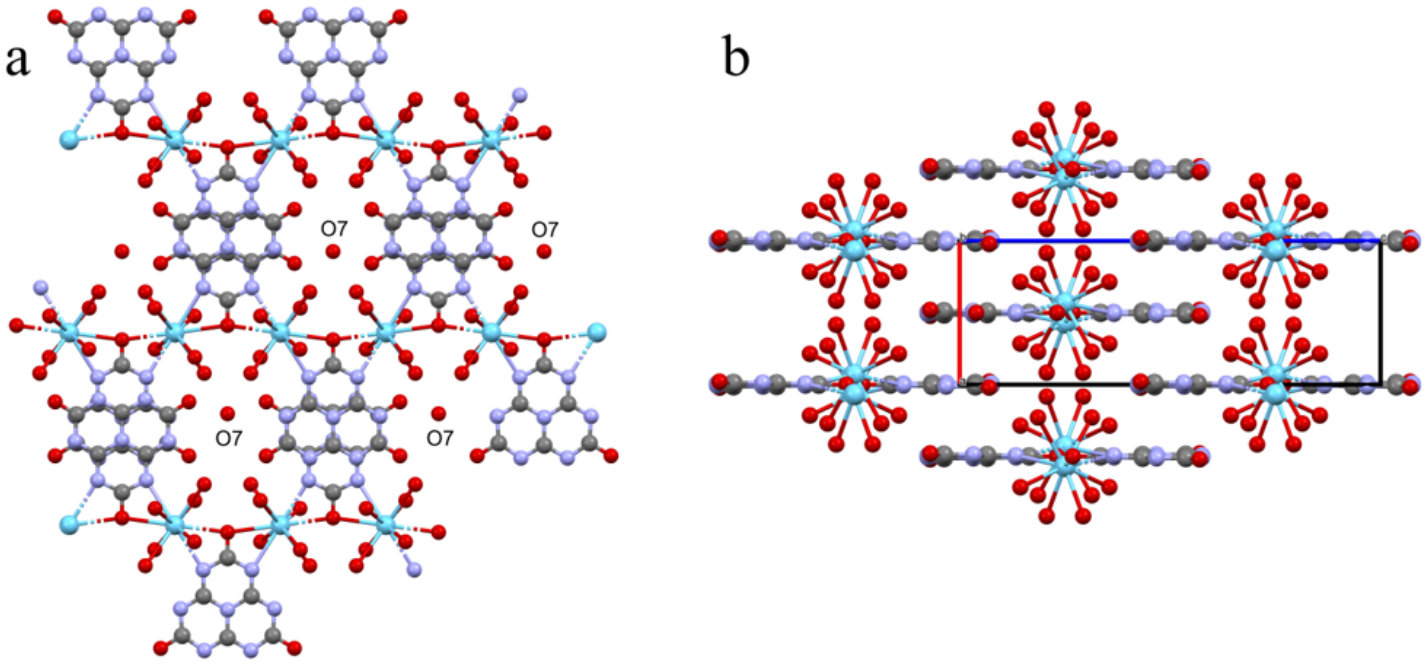

Figure 8

Endless ribbons in La2 structure (a, b). Projection along the b axis (b). Hydrogen atoms are not shown.

Supplementary Files

This is a list of supplementary files associated with this preprint. Click to download.

- GraphicalAbstract.png
- Supplementary01.10.2021corr.doc